DUFOMap: Efficient Dynamic Awareness Mapping

Daniel Duberg, Qingwen Zhang, *Graduate Student Member, IEEE*,
MingKai Jia, *Graduate Student Member, IEEE*, and Patric Jensfelt, *Member, IEEE*

Abstract—The dynamic nature of the real world is one of the main challenges in robotics. The first step in dealing with it is to detect which parts of the world are dynamic. A typical benchmark task is to create a map that contains only the static part of the world to support, for example, localization and planning. Current solutions are often applied in post-processing, where parameter tuning allows the user to adjust the setting for a specific dataset. In this paper, we propose DUFOMap, a novel dynamic awareness mapping framework designed for efficient online processing. Despite having the same parameter settings for all scenarios, it performs better or is on par with state-of-the-art methods. Ray casting is utilized to identify and classify fully observed empty regions. Since these regions have been observed empty, it follows that anything inside them at another time must be dynamic. Evaluation is carried out in various scenarios, including outdoor environments in KITTI and Argoverse 2, open areas on the KTH campus, and with different sensor types. DUFOMap outperforms the state of the art in terms of accuracy and computational efficiency. (See https://kth-rpl.github.io/dufomap for more details.)

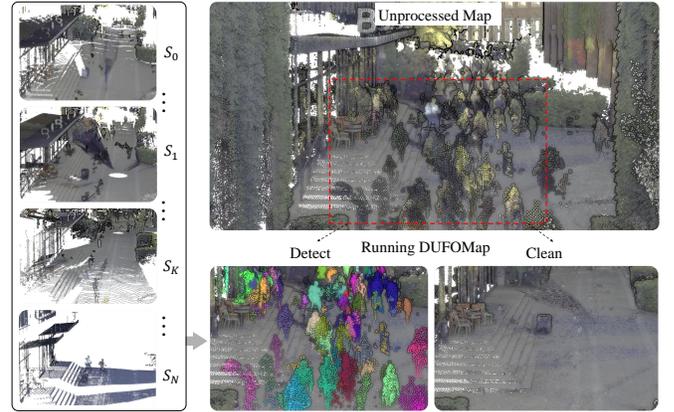*Index Terms*—Mapping; Object Detection, Segmentation and Categorization; Robotics and Automation in Construction

Fig. 1: The mapping pipeline integrates all point clouds into a global map, which initially contains numerous dynamic points. The unprocessed map is shown in the upper right. After processing with DUFOMap, the algorithm effectively detects and removes dynamic points, resulting in a clean and refined map suitable for downstream tasks.

I. INTRODUCTION

POINT clouds are a widely used representation in robotics, acquired by sensors such as LiDARs and depth cameras. Point cloud representations also find applications in other domains, e.g., surveying, architecture, and the construction industry.

Many core components in robotics assume that the environment is static. When this assumption is broken, the robot is often unable to complete its task or, at least, the efficiency is decreased. In path planning, dynamics might be misinterpreted as being part of the environment's structure, leading to unnecessarily long or convoluted paths or even failure. Dynamic objects incorrectly added to a static map or parts incorrectly removed may also reduce the robustness of localization by introducing ambiguous features or misleading the matching process. To achieve robust operation, the system needs dynamic awareness. Today, industrial mapping for

global planning and localization is, therefore, typically done offline and under human supervision.

An example from surveying where dynamic objects cause problems is shown in Fig. 1. A point cloud model of the built environment is acquired using a 3D laser scanner (Leica-RTC360). By carefully aligning the individual point clouds using artificial reference points, an accurate model can be created. Such a model is often used as a ground truth model for SLAM [1], [2]. However, as seen in the top right, the quality of the map is severely compromised by the presence of people moving around.

In this work, we look at classifying points as either static or dynamic. The main evaluation task is map cleaning, where we want to remove the points originating from moving objects and keep the rest in a point cloud map. An example of this is shown at the bottom of Fig. 1 where the dynamic points from above have been detected (left) and removed (right).

Several methods are proposed for this. Learning-based methods [3]–[6] require training data and often lack explainability. In contrast, methods based on geometric analysis, such as ray casting and visibility [7]–[10], often do not support online execution, as they rely on prior maps for difference calculations, and are computationally and memory expensive. Furthermore, they often require parameter tuning for each new setting.

In some cases, it is important to remove dynamic objects in real-time. For example, local planning cannot only rely on pre-defined maps, as the environment might change during a

Daniel Duberg, Qingwen Zhang, and Patric Jensfelt are with the Division of Robotics, Perception, and Learning (RPL), KTH Royal Institute of Technology, Stockholm 114 28, Sweden. (email: dduberg@kth.se; qingwen@kth.se; patric@kth.se)

MingKai Jia is with Robotics Institute, The Hong Kong University of Science and Technology, Hong Kong SAR, China. (email: mjiaab@connect.ust.hk)

mission. This rules out methods that rely on first acquiring all sensor data to build a global map before any cleaning happens.

In this work, we propose DUFOMap, a dynamic awareness method based on UFOMap [11]. The core of the method operates on point clouds which are processed in the voxel structure of UFOMap. Ray casting is used to identify the so-called *void* regions that at some time were empty. The classification of dynamic points can then be done by looking for points that fall into these void regions. Special care is required to account for localization errors and sensor noise. DUFOMap can be used for both offline map cleaning and online detection of dynamic points. In the offline mode, the classification of dynamic points is performed at the end based on all void regions.

We present extensive experimental validation across multiple datasets, sensors, and scenarios, showing the generality, computational efficiency, and broad usability of DUFOMap. Our approach is open-source at https://github.com/KTH-RPL/dufomap. The main contributions of our work:

- We propose a method for detecting dynamics by finding parts of space that has been observed as free taking into account sensor noise and localization errors.
- Our method achieves state-of-the-art performance in both offline and online scenarios across different scenarios and sensors.
- We demonstrate that our method generalizes in experiments on datasets with five different sensors using the same setting for the method's three parameters.

II. RELATED WORK

Dynamic awareness algorithms can be broadly categorized into learning-based and geometric analysis methods.

A. Learning-Based Methods

Learning-based methods, such as detection and segmentation in point clouds, typically involve deep neural networks and supervised training with labeled datasets. Once trained, these models are capable of inference in real-world scenarios given similar sensor settings.

Mersch *et al.* [3], Sun *et al.* [4], and Toyungyernsub *et al.* [5] develop novel frameworks to extract features and detect dynamic points utilizing spatial and temporal information. Some of these methods use the point cloud format, while others choose to translate point clouds into different representations, such as residual images, to facilitate processing. Huang *et al.* [12] propose a novel method for unsupervised point cloud segmentation by jointly learning the latent space representation and a clustering algorithm using a variational autoencoder. Lastly, Khurana *et al.* [13] use differentiable ray casting to render future occupancy predictions into future LiDAR sweep predictions for learning, allowing geometric occupancy maps to decouple the motion of the environment from the motion of the ego vehicle.

Despite the popularity of learning-based methods, they face several challenges, including the need for extensive labeled datasets, handling unbalanced data during training [14] and hard to adapt them to different operation conditions (such as
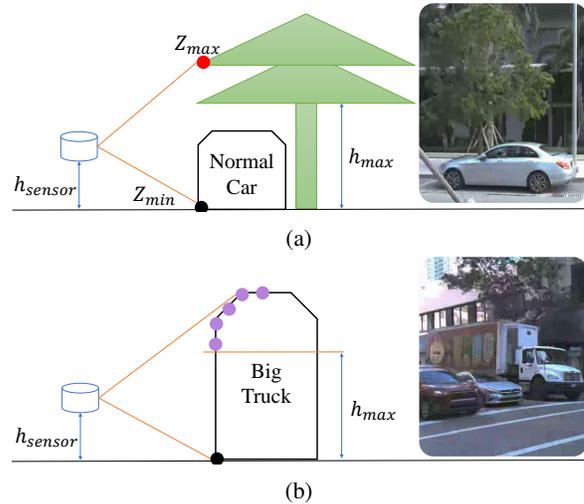

Fig. 2: Limitations of height threshold. (a) When an object is under, for example, a tree, using a height threshold h_{max} typically ignores the tree's highest points (the red point). (b) However, when choosing a threshold h_{max}, larger objects, such as a truck, may still have remaining points (purple points). Two real-world images captured from Argoverse 2 datasets demonstrate these limitations in practice.

sensors and environments). Additionally, these methods often lack explainability, making it difficult to specify the precise reasons behind poor performance in specific cases. As a result, robustness and generalization continue to be common concerns for learning-based approaches.

B. Geometric Analysis Methods

Geometric analysis methods do not require labeled data. One way to divide these methods (as in [9]) is into ray-casting and visibility-based methods. Another distinction can be made between methods that operate after all data has been acquired and, therefore, are limited to offline use and methods that can detect dynamic points (and remove them if cleaning is the task) online.

Two of the most popular post-process methods are Removert [8] and ERASOR [9] with its follow-up ERASOR2 [15]. They first build a map from all the point clouds and are thus confined to offline operation. Removert [8] projects the map into range images at the location of each query scan. Dynamic points are found based on visibility constraints by comparing query and map range images and using voting. To reduce the number of false positives, range images at decreasing resolution are used to revert dynamic points back to being static.

To address challenges when the angle between the ray and the ground is small, leading to mislabeling of ground points, Lim *et al.* [9] detect dynamic points by assuming that dynamic objects are on the ground. They compare the ratio between the min and max z values in the regions between a query scan and the map. If the ratio is larger than a threshold, then this region contains dynamics, and they remove the full bin. This design makes the method sensitive to the sensor height

and the parameters that define minimum and maximum height ranges. As a result, each new scenario typically requires a different set of parameters. Furthermore, the method struggles with overhanging objects such as trees, as shown in Fig. 2.

Occupancy grids, such as OctoMap [16] and UFOMap [11], use ray casting to update the occupancy values of the voxels in a 3D grid. This results in an estimate of the probability of each voxel being occupied over time. Points that fall into cells with an occupancy probability above some threshold are considered static. Both offline and online operations are possible. For online execution, the classification of a point is performed when the point is acquired.

The truncated signed distance field (TSDF) is an alternative to occupancy. The work closest to ours is Dynablox [17], which uses Voxblox [18] to build a TSDF. So called 'ever-free' regions are identified by setting a threshold on the TSDF values of voxels during sequential data updates. It detects dynamics as points falling into these 'ever-free' regions. Dynablox [17] runs online in a sliding window.

C. Summary

Both geometric analysis and learning-based approaches have their advantages and limitations. Robustness and generalization are common issues in learning-based methods; most importantly, they require large pre-labeled training datasets, which can be labor-intensive and time-consuming to create. State-of-the-art geometric analysis methods are typically operated offline and can therefore afford to have parameters that might need changes per scenario. Our proposed method, DU-FOMap, is designed for online dynamic awareness mapping where tuning parameters for different scenarios is not possible, but, as will be demonstrated, outperforms offline methods.

III. METHOD

Following earlier work [19], the underlying idea behind our proposed approach is to identify empty regions of space, rather than directly identify dynamic regions. The key insight is that if a region has been observed as empty at one time, points observed inside this region at another time have to be dynamic. We call a region that has been observed empty at least once a *void* region.

DUFOMap, being an extension of UFOMap [11], discretizes the world into voxels. Each voxel contains a flag i_{void} indicating whether the voxel has been observed empty at some time. Initially, i_{void} is *false* for each voxel; the i_{void} is changed to *true* when the voxel has been observed empty. A point in space is classified as static or dynamic by looking at the i_{void} flag for the corresponding voxel.

In this work, we assume that the input is pairs of sensor poses and point clouds (see Fig. 3(a)). The sensor pose is the position and orientation of the sensor in the world frame. There are no assumptions about the structure of the point clouds allowing for, for example, non-repetitive scanning patterns.

A. Classifying Void Regions

The classification of the void regions differs from the *free space* used in, for example, occupancy grids. Occupancy grids

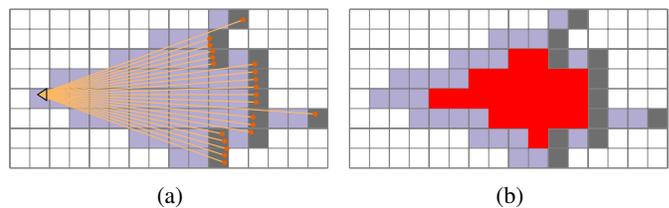(a)   (b)

Fig. 3: Example of point cloud integration in DUFOMap (shown as a single slice of the 3D grid). (a) From the sensor position, the triangle to the left, ray casting (orange lines) is performed for each point (orange dot) in the point cloud. All cells intersecting a ray are marked as intersected (purple), and the cells where a point falls within are marked as hit (gray). Unknown cells are white. (b) Cells that are intersected and surrounded exclusively by other intersected or hit cells are classified as void regions (red).

often employ a probabilistic model that updates a region based on all observations of that region. In an occupancy grid, the same part of the space can switch between being identified as free and occupied. In our work, a void region is classified as such from a single point cloud observation.

Classifying void regions from single observations, rather than accumulating evidence over time, means that a region can be classified quickly; but also that great care must be taken to prevent misclassifications. Each region is represented by a voxel, which is classified as void if it has been observed to be completely empty at least once.

To identify candidate void voxels, ray casting is performed from the sensor position to each point in the point cloud. After casting the rays, a voxel can be in one of three states (see Fig. 3(b)): *hit* (gray) if a point fell inside the voxel, *intersected* (purple) if the voxel was intersected by a ray and no point fell into it, and *unknown* (white) otherwise. The candidate void voxels are those in the intersected state.

However, a single ray intersecting a voxel does not mean that the whole voxel has been observed; therefore, it is not guaranteed to be a void voxel based exclusively on this. To this end, we propose looking at the neighboring voxels. We define the voxel in question to be fully observed given the capabilities of the sensor in use if all 26 surrounding voxels in 3D (or 8 in 2D as in Figs. 3 and 4) are also in the intersected or hit state (illustrated in red in Fig. 3(b)). Given this requirement, the voxels at the borders of the volume spanned by the point cloud cannot be confirmed to be void, as they neighbor unknown voxels.

B. Dealing With the Real World

In the real world, sensor noise and localization errors become a problem. First, we consider the problem related to localization accuracy. As mentioned and as in other works, we assume that the sensor pose is given. If the sensor pose is offset from the true pose, the hits and intersected voxels would also be offset, and, by extension, the set of classified void voxels risk being incorrect. An illustration of this problem is shown in Fig. 4(a), where the true pose is one voxel above
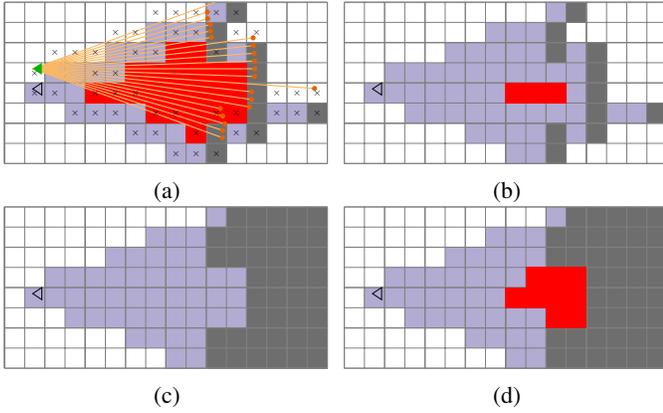
Fig. 4: Example of integration with larger localization errors (shown as a single slice of the 3D grid). (a) Point cloud with the real sensor position (green) offset one cell up compared to Fig. 3(a), showing that some cells are now incorrectly classified (x). (b) By increasing the number of neighboring cells that must be intersected or hit to two (i.e., $d_p = 2$) we account for a localization error of up to two voxels in any direction. This leads to a more conservative classification of void regions (red) compared to Fig. 3(b). (c) Extending the hits away from the sensor to allow classification of void regions next to obstacles (shown in (d)).

the estimated pose. The voxels marked with a cross correspond to voxels that would have changed state given the true pose.

To alleviate this problem, we propose to look not only at the direct neighbors of a voxel, but also at the surrounding voxels at a Chebyshev distance of d_p away; where d_p is proportional to the localization error. Setting $d_p = 2$ in the example shown in Fig. 3(a), results in the void classified voxels seen in Fig. 4(b).

From Fig. 4(b), it is observed that it is now impossible to classify voxels next to hits as void. To deal with this, anything after a hit is also considered a hit (see Fig. 4(c)). This is implemented by extending the ray casting by inserting hits from where the original ray casting ended. The voxels classified as void after this can be seen in Fig. 4(d).

Lastly, we consider the problem of sensor noise. We modeled sensor noise by marking voxels at a distance d_s ahead of the hit along the ray as hits. The value of d_s could depend on the uncertainty of the sensor range per point. In our work, we used a fixed value of d_s.

C. Classifying Points as Dynamic or Static

The majority of the computations in DUFOMap are associated with the classification of void regions, which is performed once for each new point cloud when it arrives. In contrast, classifying points as static or dynamic requires only a quick lookup of the map. If a point falls into a void voxel (that is, a voxel with $i_{void} = $ true), it is dynamic, otherwise static. This can be done at any time. By querying as a post-processing step, one benefits from all the information. This is how the map cleaning task is typically done and what we do in the following experiments. In the experiments, we also present DUFOMap*,

which runs online. Here, each new scan is classified using the map that has been built up until that time, whereas DUFOMap can make this decision using a map containing all scans.

IV. EXPERIMENTAL SETUP

We compare our method with the current state-of-the-art represented by Removert [8], ERASOR [9], OctoMap [16] and Dynablox [17]. The first three are evaluated in post-processing mode against DUFOMap. Dynablox is an online method and is compared to DUFOMap*.

A. Datasets

To demonstrate that our method can handle a wide range of scenarios and sensor types, we go beyond the use of a dataset with a single sensor type. To achieve this, we follow the benchmark evaluation protocol presented in [10]. The benchmark includes the KITTI dataset [20] with annotation labels and poses from SemanticKITTI [21]. We present results on sequences 00 and 01 in the paper. These comprise a small town and a highway, respectively, and are captured with a HDL-64E LiDAR. For other KITTI sequences, we refer to our project page https://kth-rpl.github.io/dufomap. Another dataset [22] collected by two VLP-32C LiDAR sensors is 'Argoverse 2 big city' includes various dynamic objects in an urban environment. The most sparse one is collected by a 16-channel LiDAR in a highly structured ('Semi-indoor') environment as illustrated in Fig. 5.

An additional four datasets are used in the qualitative analysis of DUFOMap. We use part of the MCD VIRAL [23] dataset. It is captured by a Leica RTC360 3D laser scanner commonly used in surveying, where the removal of dynamic objects is also highly relevant. It showcases DUFOMap's ability to handle data captured at discrete locations with significant height differences and relatively far apart rather than in a continuous stream as when driving. The data is also very dense (1.3 million points per scan vs 0.1 million for the 64-channel LiDAR) and the sensor has a much larger vertical field of view ($300°$ vs. $30°$).

To showcase the robustness and generalization of our method, we demonstrate our removal performance under highly dynamic and complex environments in Section V-B2 using datasets collected by a 128-channel LiDAR in a train station and Livox Mid-360 [24] in a two-floor structure. Additionally, small-scale experiments are also presented on our project page where we introduce two datasets captured using a RGB-D sensor.

B. Metric

Our evaluation metrics from [10] include static accuracy (SA %), dynamic accuracy (DA %), and associated accuracy (AA %) at a point level without downsampling the ground truth map to have an accurate and fair evaluation. SA represents the proportion of correctly labeled static points, while DA represents the proportion of correctly labeled dynamic points. $AA = \sqrt{SA \times DA}$ gives an overall assessment of the algorithm's performance, sensitive to doing well on both SA and DA.

TABLE I: Quantitative comparison of dynamic points removal in point cloud maps. DUFOMap⋆, results where we query for each new scan online, using the information acquired so far. The best results are shown in **bold** and the second best results are shown in underlined. Results are in percentage.

	KITTI small town (00)			KITTI highway (01)			Argoverse 2 big city			Semi-indoor		
Methods	SA ↑	DA ↑	AA ↑	SA ↑	DA ↑	AA ↑	SA ↑	DA ↑	AA ↑	SA ↑	DA ↑	AA ↑
Removert [8]	99.44	41.53	64.26	97.81	39.56	62.20	98.97	31.16	55.53	99.96	12.15	34.85
ERASOR [9]	66.70	98.54	81.07	98.12	90.94	94.46	77.51	99.18	87.68	94.90	66.26	79.30
OctoMap [16]	68.05	99.69	82.37	55.55	99.59	74.38	69.04	97.50	82.04	88.97	82.18	85.51
DUFOMap (Ours)	97.96	98.72	**98.34**	98.09	94.20	**96.12**	96.67	88.90	92.70	99.64	83.00	**90.94**
Dynablox [17]	96.76	90.68	93.67	96.33	68.01	80.94	96.08	92.87	**94.46**	98.81	36.49	60.05
DUFOMap⋆ (Ours)	98.37	92.37	95.31	98.48	81.34	89.50	98.66	73.98	85.43	99.94	54.76	73.98

C. Parameter Settings

To demonstrate our ability to handle different scenarios and sensors in an online setting, where tuning is not possible, we used the same parameter settings for DUFOMap in all experiments where otherwise not stated: voxel size $0.1\,\mathrm{m}$, $d_s = 0.2\,\mathrm{m}$ for sensor noise, and $d_p = 1$ for subvoxel localization errors. The same voxel size ($0.1\,\mathrm{m}$) was used for the other methods.

For Removert, ERASOR, and OctoMap, we used the parameters from [10]. Meaning, Removert [8] and ERASOR [9] use per-dataset optimized parameters. For Dynablox, we found that the same parameter values, slightly modified from the authors' suggestions, worked well for all experiments.

D. Hardware

Experiments were carried out on a desktop equipped with an Intel Core i9-12900KF. To assess real-time robot applicability, we also performed experiments on a robot equipped with an Intel NUC with an Intel Core i7-8559U.

V. EXPERIMENTS

A. Quantitative Evaluation

1) Accuracy: In Table I, we see that Removert does well in classifying static points (high SA) but struggles to find dynamic points in all datasets (DA $20-40\,\%$). In contrast, both ERASOR and OctoMap detect dynamic points much better, but at the cost of somewhat lower static accuracy, potentially leading to the loss of crucial map features. Our proposed method, DUFOMap, gets high scores on both SA and DA by accurately detecting dynamic points. This enables the generation of complete and clean maps for downstream tasks. The exception is Argoverse 2 where DUFOMap is only the second best for AA and trades the highest value of SA for a slightly lower DA.

Looking at the online methods, we see that, as expected, DUFOMap⋆ performs worse than DUFOMap, which has access to all data before classification is performed. Also, as expected, the performance drop is the smallest in the dataset with the least complex dynamics (KITTI small town). Dynablox does the best on the Argoverse 2 dataset where dynamic objects are constantly moving.

Both online methods have low DA for the semi-indoor dataset. One of the two people is standing still at the beginning of the dataset and both are still later (see Fig. 5(d)).

TABLE II: Runtime comparison of different methods.

Methods	Run time per point cloud [s] ↓	
	KITTI highway	Semi-indoor
Removert [8]	0.134 ± 0.004	0.515 ± 0.024
ERASOR [9]	0.718 ± 0.039	0.064 ± 0.011
OctoMap [16]	2.981 ± 0.952	1.048 ± 0.256
Dynablox [17]	0.141 ± 0.022	0.046 ± 0.008
DUFOMap (Ours)	$\mathbf{0.062 \pm 0.014}$	$\mathbf{0.019 \pm 0.003}$

DUFOMap⋆ sees these points as dynamic as soon as the person moves for the first time. Dynablox requires the person to move within a time window to detect it as dynamic.

Overall, we find that most methods have comparably lower results on the semi-indoor dataset with sparse LiDAR data.

Across all scenarios and sensor types in various datasets, DUFOMap consistently outperformed the other methods, achieving the highest AA scores and the highest or similar SA and DA scores as the best.

2) Execution Time: Table II presents information on the run time of the different methods for two of the datasets, one with a 64-channel LiDAR (KITTI highway) and one with a 16-channel LiDAR (semi-indoor). The reported time is the total processing time divided by the number of point clouds. Note that this is mainly important for the three latter methods, for which an online mode is supported. However, we see that OctoMap is prohibitively slow, requiring $3\,\mathrm{s}$ to integrate a single frame in KITTI.

In the case of the sparse LiDAR (semi-indoor), most methods operate faster due to the reduced number of points in a single scan ($64 \to 16$) and the shorter sensor range. In general, our method outperforms other methods in both dense and sparse sensor settings.

Inspired by Dynablox [17], we also performed a test on a low-power computer commonly found on robots (an Intel® NUC, see Section IV-D). We used the Dynablox setup and reduced the range to $20\,\mathrm{m}$. DUFOMap maintained a frequency of $20\,\mathrm{Hz}$ on the 4-core CPU on the semi-indoor dataset. In comparison, Dynablox operated at less than $10\,\mathrm{Hz}$.

B. Qualitative Results

In this section, we analyze the performance of our method on additional datasets to demonstrate that our method is

TABLE III: Quantatitive analysis of the influence of pose estimation by different SLAM algorithms for dynamic object removal on KITTI Sequence 00.

Methods	GT poses of KITTI [20]			SuMa [21], [25]			KISS-ICP [26]		
	SA ↑	DA ↑	AA ↑	SA ↑	DA ↑	AA ↑	SA ↑	DA ↑	AA ↑
Removert [8]	99.18	41.71	64.32	99.44	41.53	64.26	99.55	41.45	64.23
ERASOR [9]	63.83	98.35	79.23	66.70	98.54	81.07	67.86	98.68	81.83
Octomap [16]	54.81	99.56	73.87	68.05	99.69	82.37	62.28	99.85	78.85
Dynablox [17]	95.50	89.34	92.37	96.76	90.68	93.67	98.31	90.97	94.57
DUFOMap (Ours)	92.57	98.52	**95.50**	97.96	98.72	**98.34**	99.33	98.73	**99.03**

(a) Ground Truth   (b) ERASOR [9]   (c) OctoMap [16]   (d) Dyanblox [17]   (e) DUFOMap (Ours)
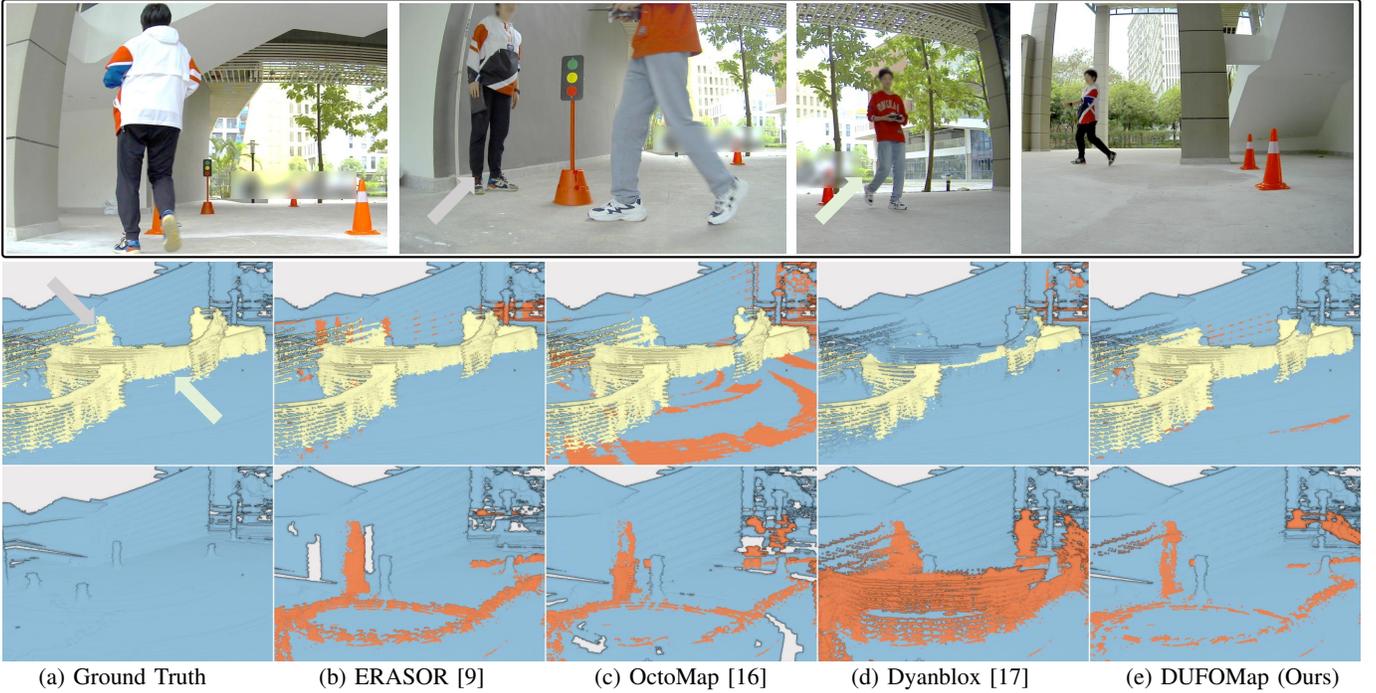
Fig. 5: Qualitative results from a self-collected dataset with a sparse LiDAR sensor (VLP-16). Points labeled as true positives are colored yellow, whereas incorrectly classified points are colored orange. The first column provides ground truth labels obtained by human annotation. The third row presents the clean map output from different methods, with orange marking any remaining dynamic points in the output map.
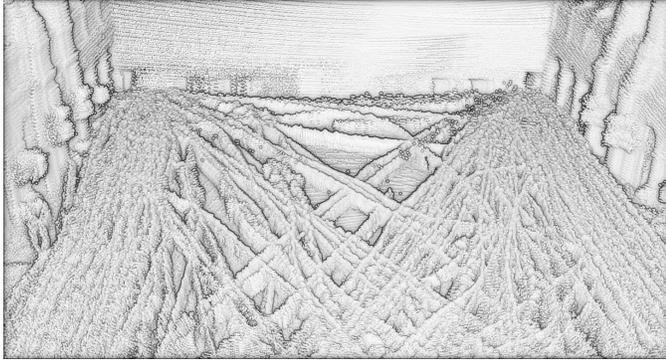
capable of handling different sensors and scenarios. Note that we use the same setting for the parameters as in previous experiments.

In the semi-indoor environment (Fig. 5), two people move around the sensor. It was harder to find good height thresholds for ERASOR in this scenario. We can see some points belonging to heads and feet still remaining. OctoMap has problems with the sparse LiDAR data (16 channels), where rays occasionally penetrate the ground, and thus to erroneous removal. The ground in their output map displays LiDAR ring-like gaps. Dynablox's performance on this dataset is markedly worse. Especially the dynamic accuracy is low, which is clearly visible as a few yellow points in the second row (few true positives) and many orange points in the third (many false negatives). Like in the previous scenario, DUFOMap gives the best output with high accuracy in both dynamic and static parts. Accounting for sensor noise and some localization errors allows DUFOMap to handle the issues faced by OctoMap regarding the ground points and to accurately identify void regions and thus dynamic points.

1) Highly Dynamic and Complex Environments: In Fig. 6, results are shown from the Urban Dynamic Objects LiDAR (DOALS) Dataset [27], which is collected in a highly dynamic train station environment. After DUFOMap processing, we get a nicely cleaned map even in this complex and highly dynamic environment.

Figure 7 shows a scene from a two-floor building that challenges methods that make assumptions about the height, the ground level, etc. DUFOMap is able to effectively remove dynamic points.

2) Survey Sensor Dataset: Our method is capable of removing the dynamic points from the Leica dataset, seen in Fig. 1. The dataset is difficult for the other methods. The following is an analysis based on the theory of the other methods to unravel these difficulties. The probabilistic model of OctoMap suffers from the few samples per voxel. For ERASOR, the height threshold would have to be automatically adjusted or redefined to handle the height differences. In a driving scenario on horizontal ground with a fixed sensor height, a fixed threshold can give very good results. However, as the height of both
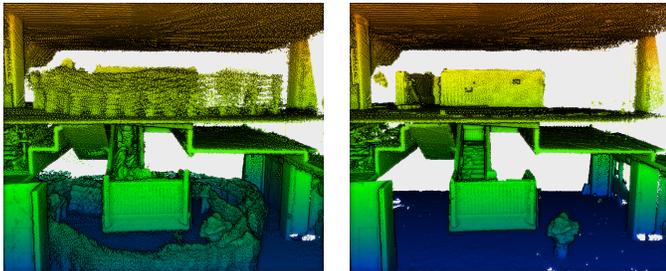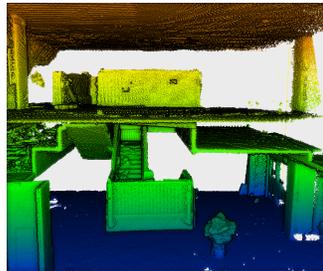
(a) Raw (Unclean) Map

(b) Cleaned Map

Fig. 6: DUFOMap dynamic points removal performance on DOALS Dataset [27] (highly dynamic environment).

(a) Raw (Unclean) Map   (b) Cleaned Map

Fig. 7: DUFOMap dynamic points removal performance in a complex, two-floor, structure. The color indicates different heights. For clearer visualization, parts of the walls have been removed.

the ground and from which the data is captured changes, as in surveying data, a fixed threshold is no longer possible. Dynablox cannot handle non-sequential data.

The output of our method is depicted in Fig. 1 (lower right) when applied to the raw data (upper). In the detection results (lower left), we naively clustered the points so that different objects stand out. For a comprehensive view of our results, readers are encouraged to visit our project page[1] where a detailed video of the entire process is available for viewing.

---

[1]https://kth-rpl.github.io/dufomap

TABLE IV: Ablation study of DUFOMap. v voxel size [m].

Parameter settings	SA [%] ↑	DA [%] ↑	AA [%] ↑
w/o d_s, d_p, $v = 0.1$	14.89	99.99	38.58
$d_s = 0.2$, $v = 0.1$	30.29	99.99	55.03
$d_p = 1$, $v = 0.1$	91.89	98.97	95.37
$d_s = 0.2$, $d_p = 1$, $v = 0.2$	92.97	98.24	95.57
$d_s = 0.2$, $d_p = 1$, $v = 0.1$	97.96	98.72	**98.34**

C. Influence of Pose Estimation

In this section, we study how the pose influences the results. We investigate three different sources of pose estimates. The KITTI dataset comes with poses that are used as ground truth in the KITTI odometry benchmark. The ground truth poses of the SemanticKITTI dataset are estimated by SuMa [25]. The third method is KISS-ICP [26]. In Table III we can see that all methods are influenced by the pose. With worse pose estimates, the scenes will appear more dynamic. Therefore, it will be more difficult to classify the static part, and we would expect SA to decrease with increased pose errors. Based on this, KISS-ICP provides more accurate and consistent pose estimates for the short sequences used in the benchmark, closely followed by the ground truth pose of SemanticKITTI (SuMa).

D. Ablation Study

In this section, we will look at how the parameters corresponding to the localization error (d_p) and the sensor noise (d_s) influence the behavior.

In our early experiments, we noted that many methods struggle (not surprisingly) to correctly classify the points on the border between what is static and what is dynamic. A person's feet touching the ground is a common and challenging example. In earlier versions of our algorithm, we used clustering to address this problem. We later find that we achieve a more accurate and general solution by better modeling the data, capturing localization errors with d_p and sensor noise with d_s. In Table IV we present the results from an ablation study on the KITTI sequence 00 where we turn on and off the sensor noise and localization error models controlled by the d_p and d_s parameters. The results clearly show how important it is to correctly classify the void regions, which is the foundation of our method. When we do not model the errors, more points will be incorrectly classified as dynamic (DA increases). In the first row, we see an extreme example where the static map is almost empty (very low SA). We can also see that accounting for localization errors (with d_p) has the greatest impact. This is because it affects the classification along the whole ray, whereas the sensor noise model mainly affects regions close to the hit.

E. Limitations

While we can operate on a large number of scenarios and sensors with the same parameter settings, there are limitations. When the LiDAR data is sparse, our conservative model for classifying void regions leads to lower dynamic accuracy. We

require a certain density to ensure that neighboring voxels are observed. This is seen in both the semi-indoor dataset (16-channel) and Argoverse 2 (32-channel but very long distances). Based on our void space classification strategy, our method must see at least the region as void once to determine that the points inside the region are dynamic. This may lead to limitations that, for a big bus moving slowly, part of the points may not be classified as dynamic. To remedy the limitations mentioned above, we can involve clustering [28] or integrate with learning-based detection [29] or scene flow estimation [30] to improve the whole pipeline in future work.

VI. CONCLUSION

In this work, we have presented DUFOMap as a dynamic awareness method based on UFOMap. Dynamics is identified implicitly by classifying empty regions of the environment. DUFOMap was evaluated against four state-of-the-art methods, in multiple different scenarios, and with a variety of sensors, showing the best overall performance.

ACKNOWLEDGMENT

REFERENCES

[1] L. Zhang, M. Helmberger, L. F. T. Fu, D. Wisth, M. Camurri, D. Scaramuzza, and M. Fallon, "Hilti-oxford dataset: A millimeter-accurate benchmark for simultaneous localization and mapping," *IEEE Robotics and Automation Letters*, vol. 8, no. 1, pp. 408–415, 2023.

[2] J. Jiao, H. Wei, T. Hu, X. Hu, Y. Zhu, Z. He, J. Wu, J. Yu, X. Xie, H. Huang *et al.*, "Fusionportable: A multi-sensor campus-scene dataset for evaluation of localization and mapping accuracy on diverse platforms," in *IEEE/RSJ International Conference on Intelligent Robots and Systems*. IEEE, 2022, pp. 3851–3856.

[3] B. Mersch, X. Chen, I. Vizzo, L. Nunes, J. Behley, and C. Stachniss, "Receding moving object segmentation in 3d lidar data using sparse 4d convolutions," *IEEE Robotics and Automation Letters*, vol. 7, no. 3, pp. 7503–7510, 2022.

[4] J. Sun, Y. Dai, X. Zhang, J. Xu, R. Ai, W. Gu, and X. Chen, "Efficient spatial-temporal information fusion for lidar-based 3d moving object segmentation," in *IEEE/RSJ International Conference on Intelligent Robots and Systems*, 2022, pp. 11 456–11 463.

[5] M. Toyungyernsub, E. Yel, J. Li, and M. J. Kochenderfer, "Dynamics-aware spatiotemporal occupancy prediction in urban environments," in *IEEE/RSJ International Conference on Intelligent Robots and Systems*, 2022, pp. 10 836–10 841.

[6] B. Mersch, T. Guadagnino, X. Chen, I. Vizzo, J. Behley, and C. Stachniss, "Building Volumetric Beliefs for Dynamic Environments Exploiting Map-Based Moving Object Segmentation," *IEEE Robotics and Automation Letters*, vol. 8, no. 8, pp. 5180–5187, 2023.

[7] J. Schauer and A. Nüchter, "The peopleremover—removing dynamic objects from 3-d point cloud data by traversing a voxel occupancy grid," *IEEE Robotics and Automation Letters*, vol. 3, no. 3, pp. 1679–1686, 2018.

[8] G. Kim and A. Kim, "Remove, then revert: Static point cloud map construction using multiresolution range images," in *IEEE/RSJ International Conference on Intelligent Robots and Systems*, 2020, pp. 10 758–10 765.

[9] H. Lim, S. Hwang, and H. Myung, "ERASOR: egocentric ratio of pseudo occupancy-based dynamic object removal for static 3d point cloud map building," *IEEE Robotics and Automation Letters*, vol. 6, no. 2, pp. 2272–2279, 2021.

[10] Q. Zhang, D. Duberg, R. Geng, M. Jia, L. Wang, and P. Jensfelt, "A dynamic points removal benchmark in point cloud maps," in *IEEE 26th International Conference on Intelligent Transportation Systems (ITSC)*, 2023, pp. 608–614.

[11] D. Duberg and P. Jensfelt, "UFOMap: An efficient probabilistic 3D mapping framework that embraces the unknown," *IEEE Robotics and Automation Letters*, vol. 5, no. 4, pp. 6411–6418, 2020.

[12] S. Huang, Z. Gojcic, J. Huang, A. Wieser, and K. Schindler, "Dynamic 3d scene analysis by point cloud accumulation," in *European Conference on Computer Vision*. Springer, 2022, pp. 674–690.

[13] T. Khurana, P. Hu, A. Dave, J. Ziglar, D. Held, and D. Ramanan, "Differentiable raycasting for self-supervised occupancy forecasting," in *European Conference on Computer Vision*. Springer, 2022, pp. 353–369.

[14] Y. Zhang, Q. Hu, G. Xu, Y. Ma, J. Wan, and Y. Guo, "Not all points are equal: Learning highly efficient point-based detectors for 3d lidar point clouds," in *IEEE Conference on Computer Vision and Pattern Recognition*, 2022.

[15] H. Lim, L. Nunes, B. Mersch, X. Chen, J. Behley, H. Myung, and C. Stachniss, "ERASOR2: instance-aware robust 3d mapping of the static world in dynamic scenes," in *Robotics: Science and Systems (RSS 2023)*. IEEE, 2023.

[16] A. Hornung, K. M. Wurm, M. Bennewitz, C. Stachniss, and W. Burgard, "OctoMap: An efficient probabilistic 3D mapping framework based on octrees," *Autonomous Robots*, 2013.

[17] L. Schmid, O. Andersson, A. Sulser, P. Pfreundschuh, and R. Siegwart, "Dynablox: Real-time detection of diverse dynamic objects in complex environments," *IEEE Robotics and Automation Letters*, vol. 8, no. 10, pp. 6259 – 6266, 2023.

[18] H. Oleynikova, Z. Taylor, M. Fehr, R. Siegwart, and J. Nieto, "Voxblox: Incremental 3d euclidean signed distance fields for on-board mav planning," in *IEEE/RSJ International Conference on Intelligent Robots and Systems*, 2017.

[19] M. Lindstrom and J.-O. Eklundh, "Detecting and tracking moving objects from a mobile platform using a laser range scanner," in *IEEE/RSJ International Conference on Intelligent Robots and Systems*, vol. 3. IEEE, 2001, pp. 1364–1369.

[20] A. Geiger, P. Lenz, C. Stiller, and R. Urtasun, "Vision meets robotics: The kitti dataset," *International Journal of Robotics Research*, 2013.

[21] J. Behley, M. Garbade, A. Milioto, J. Quenzel, S. Behnke, C. Stachniss, and J. Gall, "SemanticKITTI: A dataset for semantic scene understanding of LiDAR sequences," in *IEEE/CVF International Conference on Computer Vision*, 2019.

[22] B. Wilson, W. Qi, T. Agarwal, J. Lambert, J. Singh, S. Khandelwal, B. Pan, R. Kumar, A. Hartnett, J. K. Pontes, D. Ramanan, P. Carr, and J. Hays, "Argoverse 2: Next generation datasets for self-driving perception and forecasting," in *Neural Information Processing Systems Track on Datasets and Benchmarks*, 2021.

[23] N. Thien-Minh, Y. Shenghai, N. Thien Hoang, Y. Pengyu, C. Haozhi, X. Lihua, W. Maciej, J. Patric, T. Marko, Z. Justin, and B. Noel, "Mcd: Diverse large-scale multi-campus dataset for robot perception," in *Conference on Computer Vision and Pattern Recognition*, 11 2024. [Online]. Available: https://mcdviral.github.io/

[24] "Livox Mid-360," https://www.livoxtech.com/mid-360, accessed: 2024-02-05.

[25] J. Behley and C. Stachniss, "Efficient surfel-based slam using 3d laser range data in urban environments," in *Proc. of Robotics: Science and Systems (RSS)*, 2018.

[26] I. Vizzo, T. Guadagnino, B. Mersch, L. Wiesmann, J. Behley, and C. Stachniss, "KISS-ICP: In Defense of Point-to-Point ICP – Simple, Accurate, and Robust Registration If Done the Right Way," *IEEE Robotics and Automation Letters*, vol. 8, no. 2, pp. 1029–1036, 2023.

[27] P. Pfreundschuh, H. F. Hendrikx, V. Reijgwart, R. Dubé, R. Siegwart, and A. Cramariuc, "Dynamic object aware lidar slam based on automatic generation of training data," in *IEEE International Conference on Robotics and Automation*, 2021, pp. 11 641–11 647.

[28] R. J. Campello, D. Moulavi, and J. Sander, "Density-based clustering based on hierarchical density estimates," in *Pacific-Asia conference on knowledge discovery and data mining*. Springer, 2013, pp. 160–172.

[29] MMDetection Contributors, "OpenMMLab Detection Toolbox and Benchmark," Aug. 2018. [Online]. Available: https://github.com/open-mmlab/mmdetection

[30] Q. Zhang, Y. Yang, H. Fang, R. Geng, and P. Jensfelt, "Deflow: Decoder of scene flow network in autonomous driving," *arXiv preprint arXiv:2401.16122*, 2024.